
Model Selection of Zero-shot Anomaly Detectors in the Absence of Labeled Validation Data

Clement Fung^{1*} Chen Qiu² Aodong Li³ Maja Rudolph²

Abstract

Anomaly detection requires detecting abnormal samples in large unlabeled datasets. While progress in deep learning and the advent of foundation models has produced powerful zero-shot anomaly detection methods, their deployment in practice is often hindered by the lack of labeled data—without it, their detection performance cannot be evaluated reliably. In this work, we propose SWSA (Selection With Synthetic Anomalies): a general-purpose framework to select image-based anomaly detectors with a generated synthetic validation set. Our proposed anomaly generation method assumes access to only a small support set of normal images and requires no training or fine-tuning. Once generated, our synthetic validation set is used to create detection tasks that compose a validation framework for model selection. In an empirical study, we find that SWSA often selects models that match selections made with a ground-truth validation set, resulting in higher AUROCs than baseline methods. We also find that SWSA selects prompts for CLIP-based anomaly detection that outperform baseline prompt selection strategies on all datasets, including the challenging MVTec-AD and VisA datasets.

1. Introduction

Anomaly detection, automatically identifying samples that deviate from normal behavior, is an important technique for supporting medical diagnosis (Fernando et al., 2021), safeguarding financial transactions (Ahmed et al., 2016), bolstering cybersecurity (Mirsky et al., 2018; Siadati & Memon, 2017), and ensuring smooth industrial opera-

tions (Bergmann et al., 2019). While there has been significant progress in approaches for unsupervised anomaly detection (Deecke et al., 2021; Liznerski et al., 2022; Li et al., 2023a; 2021; Reiss et al., 2021), recent developments in foundation models have made it possible to pre-train a large model on large-scale data from one domain and then to deploy it for a new anomaly detection task. In particular, zero-shot CLIP-based anomaly detection approaches (Jeong et al., 2023b; Liznerski et al., 2022; Zhou et al., 2021; Esmaeilpour et al., 2022) have shown great performance in many domains. While these approaches provide the exciting possibility to deploy anomaly detectors for new applications without training data, one must trust that they perform as well as expected before deployment. Performing such an evaluation is often hindered by a major barrier: the absence of labeled validation data. For many anomaly detection domains, validation data is absent as anomalies are rare and the large volume of available data is too expensive to label (Görnitz et al., 2013; Trittenbach et al., 2021).

In this work, we study the efficacy of generated anomalies for model selection of image-based zero-shot anomaly detectors through our proposed framework SWSA (Selection With Synthetic Anomalies). We compare two promising strategies for generating synthetic anomalies: (i) augmentation methods from prior work (Li et al., 2021) and (ii) a novel approach that leverages pre-trained diffusion models (Ho et al., 2020; Song et al., 2021; Jeong et al., 2023a). Both methods assume access to only a small set of normal examples for a given image-based anomaly detection task and does not perform any training. Generated synthetic anomalies are mixed with normal examples to create a synthetic validation dataset. When evaluating our synthetic validation datasets across 329 anomaly detection tasks, ranging from natural image domains to industrial defects, we find that SWSA often matches the selections made with real ground-truth validation sets and outperforms baseline selection strategies.

Our anomaly generation methods do not require any training, fine-tuning, or domain-specific methods for new anomaly detection tasks. Instead, we use a pre-trained ImageNet diffusion model (Deng et al., 2009; Dhariwal & Nichol, 2021) to interpolate between normal images (Jeong et al., 2023a). Our method can be applied even for image domains

* Work done during internship at Bosch Center for AI. ¹Software and Societal Systems Department, Carnegie Mellon University, Pittsburgh, USA ²Bosch Center for Artificial Intelligence, Pittsburgh, USA ³Department of Computer Science, University of California, Irvine, USA. Correspondence to: Clement Fung <clementf@cs.cmu.edu>.

that are far from ImageNet, such as images of industrial defects (Bergmann et al., 2019; Zou et al., 2022).

Our work makes the following contributions:

- In Sec. 3.1, we present SWSA: a framework for selecting anomaly detection models with synthetic anomalies. Figure 1 shows the outline of our approach.
- We propose a practical technique for generating synthetic anomalies with a general-purpose pre-trained diffusion model—without any fine-tuning or auxiliary datasets, described in Sec. 3.2. When used in SWSA, we show that these synthetic anomalies are most effective for model selection in natural settings (i.e., birds and flowers).
- We empirically evaluate SWSA on a wide range of anomaly detection tasks and demonstrate its success on two use-cases: model selection amongst candidate anomaly detectors (Sec. 4.2) and prompt selection for anomaly detection with CLIP (Sec. 4.3).

2. Related Work

Unsupervised anomaly detection. Recent advances in anomaly detection models include autoencoder-methods (Chen & Konukoglu, 2018; Principi et al., 2017), deep one-class classification (Ruff et al., 2018; 2019), and self-supervised learning-based methods (Bergman & Hoshen, 2020; Hendrycks et al., 2019b; Qiu et al., 2021; Sohn et al., 2020; Qiu et al., 2022a; Schneider et al., 2022). While these methods are unsupervised, their architectures and training frameworks involve selection of various hyper-parameters, which can have a strong impact on detection accuracy (Campos et al., 2016; Goldstein & Uchida, 2016; Han et al., 2022). While Ding et al. (2022) propose to circumvent model selection by building an ensemble of candidate methods, model selection typically requires labeled validation data.

In outlier exposure (Hendrycks et al., 2019a), which has been extended to contaminated data settings (Qiu et al., 2022b) and meta-learning (Li et al., 2023b), further improvements in detection accuracy come from fine-tuning on an auxiliary dataset, usually Tiny-ImageNet. Although these auxiliary samples provide valuable training signal, they are too dissimilar from normal samples and are easily detected, making them poor ineffective for model evaluation or selection. Work in semi-supervised anomaly detection (Görnitz et al., 2013; Das et al., 2016; Trittenbach et al., 2021; Li et al., 2023a) assumes access to a training set with some labeled anomalies but obtaining such data is unrealistic for many applications.

Zero-shot anomaly detection with foundation models. Foundation models are pre-trained on massive datasets to

learn rich semantic image features and are effective for anomaly detection in new vision domains with no additional training required, i.e. in a zero-shot manner. Examples include models such as vision transformers (ViT, (Dosovitskiy et al., 2021)) or residual networks (ResNet, (He et al., 2016)) pre-trained on ImageNet (Deng et al., 2009).

Another powerful class of foundation models are vision-language models like CLIP (Radford et al., 2021). With hand-crafted text prompts CLIP can be employed on a new anomaly detection (Liznerski et al., 2022) or anomaly segmentation tasks (Jeong et al., 2023b; Zhou et al., 2021) without training data. However, detection performance depends on the choice of prompts (Liznerski et al., 2022; Jeong et al., 2023b), which often requires labeled validation data for prompt selection. Esmaeilpour et al. (2022) use normal samples to learn a text description generator for CLIP-based out-of-distribution detection. However, when task-specific instances of foundation models require little to no data, we often cannot assume access to such labeled data.

Meta-evaluation of anomaly detection. Nguyen et al. (2016); Marques et al. (2015; 2020) propose unsupervised model selection strategies with so-called “internal metrics” computed from predicted anomaly scores on unlabeled data. Meta-training offers another set of approaches for unsupervised anomaly detector selection (Schubert et al., 2023; Zhao et al., 2021; 2022). However, since meta-learning requires a large number of related labeled datasets, their application has been limited to tabular data, and prior work on internal metrics has been applied to tabular anomaly detection only (Nguyen et al., 2016; Marques et al., 2015; 2020; Ma et al., 2023). Shoshan et al. (2023) also explore synthetic data for model selection; however, their work focuses on optimizing model training: synthetic data is used to select random seeds, select hyper-parameters, and for early stopping criteria. Shoshan et al. (2023) train a GAN to generate synthetic data, which is not applicable to our setting where we assume that data is scarce. Our work instead focuses on selecting zero-shot anomaly detection methods without any model training or fine-tuning.

Generating images with guidance. Diffusion models (Ho et al., 2020; Song et al., 2021) have recently been shown to outperform other generative models (Dhariwal & Nichol, 2021). Although generative models are traditionally used to generate in-distribution data, a variety of prior work has proposed techniques that guide generative models to generate new distributions. Specifically, text-guided generation (Kim et al., 2022; Kwon et al., 2023; Kwar et al., 2023; Mokady et al., 2023; Tumanyan et al., 2023) with CLIP (Radford et al., 2021) guides the image generation process with text prompts to generate samples from a distribution of interest, e.g. “cat with glasses”. Luo et al. (2023)

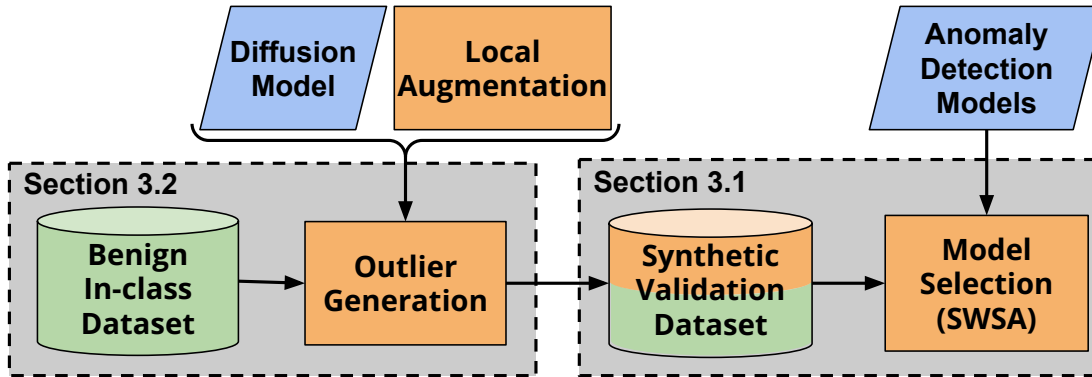


Figure 1: We propose to use two methods to generate synthetic images, as described in Sec. 3.2: image-guided generation with a diffusion model and local image augmentation. We produce a synthetic validation set containing both real normal images and synthetic images. The synthetic validation set is then used for model selection, as described in Sec. 3.1. Components in blue are frozen, components in green are real data, and components in orange are implemented methods.

use the CLIP embeddings of different class labels to guide StyleGAN (Karras et al., 2019; 2020) to generate images for classifier evaluation. Similarly, Jain et al. (2023) use CLIP for model diagnosis. These approaches require the target labels (e.g. gender, glasses, etc.) as inputs, but the nature of anomalies is typically unknown. Instead, we rely on DiffStyle (Jeong et al., 2023a), which provides training-free guidance for image generation by interpolating two images during the reverse DDIM process (Song et al., 2021). We find that interpolating between two normal samples will typically preserve dominant visual features, such as realistic textures and background, while introducing slight manipulations that make the generated images promising candidates for synthetic anomalies in SWSA.

3. Method

In this section, we propose to leverage data augmentation and diffusion-based image generation techniques to generate synthetic anomalies. By using these synthetic anomalies as a *synthetic validation dataset*, we enable model selection in the absence of a real validation dataset. We call our framework SWSA. In Sec. 3.1, we describe how synthetic anomalies are used in SWSA. We then propose our synthetic anomaly generation approaches in Sec. 3.2. Figure 1 demonstrates the overall process used in SWSA.

3.1. Model Selection with Synthetic Anomalies

The absence of labeled validation data is a major roadblock in the deployment of anomaly detection methods. However, normal data can usually be obtained. For this reason, we follow Zhao et al. (2021), and assume access to a set of normal samples we call the *support set* X_{support} . In our empirical study, we show that the support set can have as few as 10 samples. Using this support set, we construct a synthetic

validation set that can aid model selection. Creating a synthetic validation set and using it for model selection entails the following steps:

Step 1: Partitioning the support set. The support set X_{support} , is randomly partitioned into seed images X_{seed} and normal validation images X_{in} . X_{seed} is used for anomaly generation, and X_{in} is held out for evaluation.

Step 2: Generating synthetic anomalies. The seed images are processed with either DiffStyle (Jeong et al., 2023a) or CutPaste (Li et al., 2021) to produce synthetic anomalies \tilde{X}_{out} . Details will be given in Sec. 3.2.

Step 3: Mixing the synthetic validation set. The normal validation images X_{in} are combined with the synthetic anomalies \tilde{X}_{out} to produce a labeled synthetic validation set,

$$\mathcal{D} = \{(x, 1) | x \in \tilde{X}_{\text{out}}\} \cup \{(x, 0) | x \in X_{\text{in}}\}, \quad (1)$$

where label 1 indicates an anomaly and 0 a normal image.

Step 4: Evaluating detection with candidate models. In a final step, we evaluate candidate models by their detection performance on the synthetic validation set \mathcal{D} . We use AUROC, the area under the receiving operator characteristic curve, which is typically used to evaluate anomaly detection models (Emmott et al., 2015; Maxion & Tan, 2000).

Since we assume access to only a small support set, training or fine-tuning a generative (diffusion) model is infeasible. Instead, in Sec. 3.2, we propose to use (i) a pre-trained ImageNet DDIM (Song et al., 2021) and (ii) DiffStyle, a training-free method for diffusion-based image-to-image style transfer. We adapt DiffStyle to generate synthetic anomalies. We also propose to use CutPaste (Li et al., 2021), a data augmentation technique that produces local image modifications, to generate synthetic anomalies. Our applications of the diffusion-based method and CutPaste do not

perform any model training or fine-tuning and do not require any data outside of the seed set X_{seed} .

3.2. Generating Synthetic Anomalies

We propose two methods for generating synthetic anomalies: CutPaste and a diffusion-based method.

CutPaste. CutPaste (Li et al., 2021) is a data augmentation method that is used for training unsupervised anomaly detection models. To modify an image, Li et al. (2021) randomly select a cropped region of an image, and pastes it onto a different region of the image. In our work, we propose a different application for CutPaste’s data augmentation: after modifying benign, in-class images from the seed set X_{seed} , the resulting images are treated as synthetic anomalies for model selection.

Diffusion-based generation. We use DiffStyle (Jeong et al., 2023a), diffusion-based style transfer, to generate synthetic anomalies with a pretrained DDIM. We first equally divide the seed set X_{seed} into style images X_{style} and content images X_{content} . DiffStyle takes any style-content image pair $\{I^{(1)}, I^{(2)}\}$ as input—and produces a new, generated image with $I^{(2)}$ ’s content and $I^{(1)}$ ’s style. To achieve this, $I^{(1)}$ and $I^{(2)}$ are mapped into the diffusion model’s latent space through the forward diffusion process to produce latent vectors $x_T^{(1)}$ and $x_T^{(2)}$. We refer to the h-space (i.e., the inner-most layer of the UNet) of $x_T^{(1)}$ and $x_T^{(2)}$ as $h^{(1)}$ and $h^{(2)}$ respectively. h-space has been shown to be a meaningful semantic space for images, enabling linearity and composition properties, and can be manipulated during a diffusion model’s image generation process. We refer readers for more details related to h-space to Kwon et al. (2023) and Jeong et al. (2023a).

Given two latent vectors $h^{(1)}$ and $h^{(2)}$, we perform a linear interpolation: $h^{(\text{gen})} = (1 - \gamma)h^{(1)} + \gamma h^{(2)}$ where γ represents the relative strength of the content image during style transfer. We use $\gamma = 0.7$ in our experiments. We then perform the asymmetric reverse diffusion process using $x_T^{(1)}$, replacing the h-space with $h^{(\text{gen})}$:

$$x_{t-1} = \sqrt{\alpha_{t-1}}\mathbf{P}_t(\epsilon_t^\theta(x_T^{(1)}|h^{(\text{gen})})) + \mathbf{D}_t(\epsilon_t^\theta(x_T^{(1)})). \quad (2)$$

Once the reverse process is completed (i.e., at $t = 0$), the final output x_0 is saved as a synthetic anomaly. To generate the full set of synthetic anomalies \tilde{X}_{out} , we apply all possibilities of $(I^{(1)}, I^{(2)})$ in the cross product of X_{style} and X_{content} . Figure 2 shows examples of anomalies generated with this approach; we find that our generated images have realistic backgrounds and textures, but can contain various semantic corruptions expected of anomalous images. Our synthetic anomaly generation method assumes *no knowledge of the*

distribution of potential anomalies: the general-purpose diffusion model is not fine-tuned and only images from the seed set X_{seed} are used as inputs.

4. Empirical Study

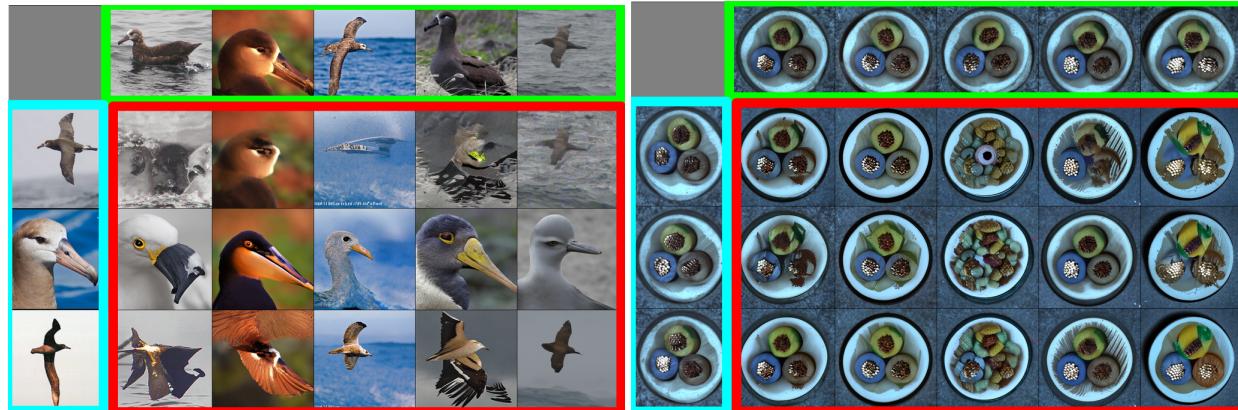
To study the efficacy of synthetic anomalies for model selection, we investigate whether SWSA selects similar models and settings as ground-truth validation sets. Our evaluation spans various vision domains, including natural and industrial images. We first describe the datasets, anomaly detection tasks, and anomaly generation details in Sec. 4.1. Next, we showcase two use cases of SWSA: model selection and CLIP prompt selection—we find that SWSA selects the true best-performing model in seven of eight cases (Sec. 4.2) and outperforms all other strategies for CLIP prompt selection (Sec. 4.3); these results are achieved without any access to the real validation data.

4.1. Experimental Setup

We present an experimental setup that can be used as a benchmark to evaluate synthetic validation data. Our benchmark uses a set of anomaly detectors and anomaly detection tasks spanning four datasets. The tasks vary by difficulty from the easier one-vs-rest to the more difficult one-vs-closest anomaly detection setting. The goal of this benchmark is to evaluate how well results on synthetic validation data correspond to results one would obtain with ground-truth validation data; we estimate the absolute detection performance, the relative ranking of anomaly detectors, and the optimal hyper-parameters (such as prompts for CLIP-based anomaly detection).

Datasets. Our benchmark spans four frequently-used image datasets: Oxford Flowers (Nilsback & Zisserman, 2008), Caltech-UCSD Birds (CUB) (Wah et al., 2011), MVTec Anomaly Detection dataset (MVTec-AD) (Bergmann et al., 2019), and Visual Anomaly Detection (VisA) (Zou et al., 2022). These datasets span both the natural image domain (Flowers and CUB) and the visual anomaly detection domain (MVTec-AD and VisA). CUB and Flowers are multi-class datasets containing 200 bird species and 102 flower species respectively. MVTec-AD and VisA contain several (i.e., 15 in MVTec-AD, 12 in VisA) real industrial product categories; for each category, the training subset contains images of defect-free products, and the testing subset contains labeled images of both good and defective products.

Anomaly detection tasks. Our benchmark contains 329 anomaly detection tasks: 15 from MVTec-AD, 12 from VisA, 200 from CUB, and 102 from Flowers. For all datasets, each class or product is treated as normal for an individual anomaly detection task. Besides considering the



(a) CUB class 1 (“Black Footed Albatross”)

(b) MVTec-AD cable

Figure 2: Examples of synthetic anomalies generated with our diffusion-based method for CUB class 1 (left) and MVTec-AD “cable” (right). For each example, the top row of images (in green) are used as source “style” images, and the left column of images (in cyan) are used as source “content” images. The inner grid (in red) shows each pairwise interpolation between the source style and content image, performed with our modified DiffStyle process. All source images are drawn from the distribution of class 1 support images; no validation data or images from other classes are used.

usual one-vs-rest anomaly detection setup for multi-class datasets CUB and Flowers, we also adopt the near-anomaly-detection setup used in Mirzaei et al. (2023) to simulate more difficult anomaly detection tasks: specifically, after individually selecting each class as the inlier class, we consider each out-class individually and report the class with the worst performance (i.e., one-vs-closest). For MVTec-AD and VisA, we predict if an image contains a defective product. Each product contains multiple types of defects; we consider all defect types as a single class for one-vs-rest and the worst-performing defect type for one-vs-closest. For all tasks, images from the in-class training subset are used as the support set, and images from the relevant in-class and out-class validation subsets are used to constructing the ground-truth validation set.

Generating synthetic anomalies. For all four datasets and all 329 anomaly detection tasks, we generate synthetic anomalies with training examples from the in-class distribution only. Both the diffusion-based method and CutPaste as used to generate the same number of images with X_{seed} . For the CUB, VisA, and MVTec-AD datasets, we sample 20 images for X_{seed} from the training set, generating 100 synthetic anomalies with each method. For the Flowers dataset, only 10 images are included in the training set for each class, so we generate 25 synthetic anomalies with each method. Figure 2 shows 15 examples of generated synthetic anomalies for a single CUB class (left) and a single MYTec-AD product (right).

Although prior results in Kwon et al. (2023) and Kim et al. (2022) suggest that a diffusion model trained in the same domain is required to generate high-quality images, we find

that using one common diffusion model can generate sufficiently effective anomalies for SWSA. We use the same pre-trained diffusion model (256x256 model trained on ImageNet without class conditioning from Dhariwal & Nichol (2021)) for all datasets and anomaly detection tasks.

4.2. Model Selection on Synthetic Data

We first demonstrate the effectiveness of SWSA for model selection. Given a set of candidate models, we show that SWSA can select the true optimal model.

Candidate anomaly detection models. We experiment across five pre-trained ResNet models (ResNet-152, ResNet-101, ResNet-50, ResNet-34, ResNet-18) and five pre-trained Vision Transformers (ViT-H-14, ViT-L-32, ViT-L-16, ViT-B-32, ViT-B-16). We use the ImageNet pre-trained model weights of Dosovitskiy et al. (2021); He et al. (2016).

Deep-nearest-neighbor anomaly detection. To perform anomaly detection, we use the nearest-neighbor-based method of Bergman et al. (2020). We use the values of a candidate model’s penultimate layer as the output of a feature extractor F and process the support set X_{support} with F to establish a feature bank Z :

$$z_s = F(x_s), \forall x_s \in X_{\text{support}} \quad (3)$$

To perform anomaly detection on an input example d , the Euclidean distance between $F(d)$ and its k -nearest neighbors in Z is used as an anomaly score s :

$$s = \sum_{z_s \in Z_k(d)} \|F(d) - z_s\|_2^2 \quad (4)$$

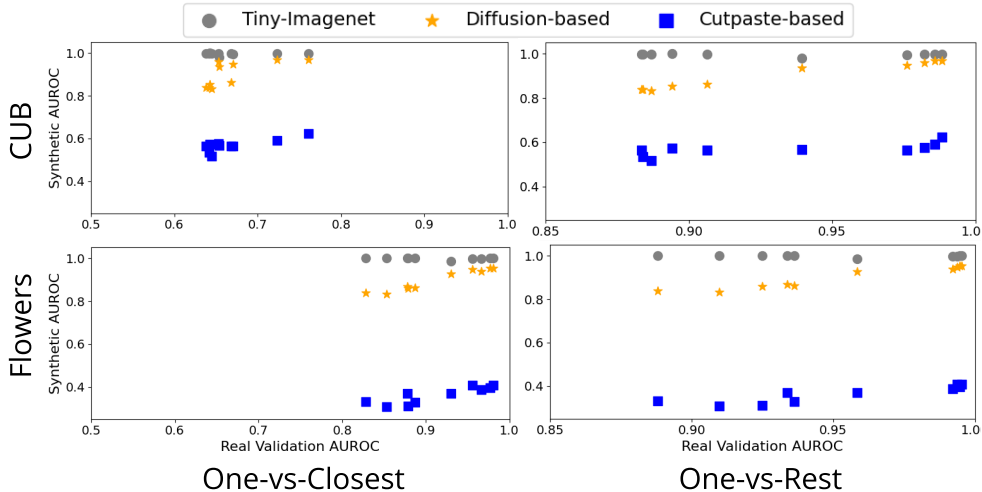


Figure 3: The real and synthetic validation AUROC is compared for the CUB and Flowers datasets, using three candidate synthetic validation sets. We observe that the real ranking of models is preserved when using diffusion-based anomalies for both datasets on the one-vs-rest anomaly detection setting.

where $Z_k(d)$ are the k -nearest neighbors to d in the feature bank. Bergman et al. (2020) find that small values of k are effective, and we use $k = 3$.

Evaluation setup. For each task, we compute the AUROC for each candidate model on both the synthetic validation and real validation datasets. For each dataset, we average the AUROC across tasks to compute the “synthetic AUROC”. We repeat this process with real validation datasets, again averaging over tasks to compute the “real validation AUROC”. To evaluate our model selection, we select the model with the best synthetic AUROC for a given task and report the selected model’s corresponding real validation AUROC. We also compare real and synthetic AUROCs to investigate if the rankings of candidate models are similar.

To establish a baseline for this evaluate, we compare SWSA using our synthetic anomalies to SWSA using the Tiny-ImageNet dataset. Hendrycks et al. (2019a) found that examples from an auxiliary dataset can be effective for outlier exposure, and we investigate if such auxiliary examples can also be effective for model selection. When sampling anomalies from Tiny-Imagenet, we sample uniformly at random to generate a dataset \tilde{X}_{out} of the same size: 100 images for tasks with CUB, VisA, and MVTec-AD; 25 images for tasks with the Flowers dataset.

Evaluation results. Table 1 shows, for different model selection strategies, both the rate at which the best model is picked and the resulting AUROC. We find that diffusion-based synthetic anomalies and CutPaste-based synthetic anomalies pick the best model at the highest rate and produce the highest AUROC for seven out of eight evaluation

settings, even outperforming the strategy that always selects the largest model (ViT-H-14). In particular, SWSA with diffusion-based anomalies selects the best model with the highest frequency for all CUB and Flowers settings.

We also consider the full model ranking beyond the selected model. Figure 3 shows the results for the CUB and Flowers (bottom) datasets, for both the one-vs-closest (left) and one-vs-rest (right) settings. In an ideal synthetic validation, the model ranking with synthetic data (along the y-axis) should match the model ranking with real data (along the x-axis). We find that SWSA with diffusion-based anomalies provides the most consistent ranking, especially for one-vs-rest tasks which are more robust to class variations. This result holds even when as few as three synthetic anomalies are used; Appendix A contains additional results and analysis. We find that the one-vs-closest benchmark, an estimate of worst-case performance, is harder to estimate with synthetic anomalies. Figure 3 shows that, although the real and synthetic AUROCs rankings are similar for the Flowers dataset, the rankings are less similar for the one-vs-closest benchmark on the CUB dataset. Finally, we find that SWSA is less effective in model ranking for the MVTec-AD and VisA datasets; we discuss potential reasons for this in Sec. 4.4 and show additional results in Appendix A. However, as shown in the next section, our synthetic validation is still extremely effective for selecting CLIP prompts for all datasets, including MVTec-AD and VisA.

4.3. CLIP Prompt Selection on Synthetic Data

The performance of CLIP-based anomaly detection models depends on the choice of prompts (Jeong et al., 2023b; Liznerski et al., 2022). Prior works evaluate candidate CLIP

Model Selection of Zero-shot Anomaly Detectors in the Absence of Labeled Validation Data

Table 1: When using synthetic anomalies for model selection, we report both the accuracy in picking the best model (“pick rate”) and the resulting AUROC. SWSA picks the best model more often and produces higher AUROCs than simply selecting the largest model for all tasks. Diffusion-based synthetic anomalies are also particularly effective for model selection on the Flowers and CUB datasets.

		Flowers		CUB		MVTec-AD		VisA	
		Pick rate	AUROC						
One-vs-Closest	Largest model	43 / 102	0.956	11 / 200	0.653	4 / 15	0.716	1 / 12	0.636
	SWSA (TinyImg)	50 / 102	0.966	30 / 200	0.674	4 / 15	0.716	1 / 12	0.636
	SWSA (Diffusion)	59 / 102	0.967	66 / 200	0.737	4 / 15	0.790	0 / 12	0.643
	SWSA (CutPaste)	37 / 102	0.945	60 / 200	0.743	2 / 15	0.678	1 / 12	0.674
One-vs-Rest	Largest model	49 / 102	0.994	32 / 200	0.982	4 / 15	0.733	1 / 12	0.765
	SWSA (TinyImg)	57 / 102	0.993	59 / 200	0.982	4 / 15	0.733	1 / 12	0.765
	SWSA (Diffusion)	62 / 102	0.994	109 / 200	0.988	2 / 15	0.678	0 / 12	0.764
	SWSA (CutPaste)	37 / 102	0.974	62 / 200	0.966	2 / 15	0.717	1 / 12	0.772

Table 2: When using our synthetic outliers for CLIP prompt selection, we report both the accuracy in picking the best prompt (“pick rate”) and the resulting AUROC. SWSA picks the best prompt most often and produces higher AUROCs than baseline prompt selection techniques for all datasets.

		Flowers		CUB		MVTec-AD		VisA	
		Pick rate	AUROC						
One-vs-Closest	Default Prompt	1 / 102	0.697	5 / 200	0.571	1 / 15	0.540	1 / 12	0.491
	Prompt Ensemble	0 / 102	0.708	0 / 200	0.577	0 / 15	0.555	0 / 12	0.494
	SWSA (TinyImg)	18 / 102	0.718	34 / 200	0.582	1 / 15	0.559	4 / 12	0.514
	SWSA (Diffusion)	38 / 102	0.729	46 / 200	0.590	3 / 15	0.529	1 / 12	0.475
	SWSA (CutPaste)	18 / 102	0.718	34 / 200	0.585	4 / 15	0.609	1 / 12	0.507
One-vs-Rest	Default Prompt	1 / 102	0.959	0 / 200	0.971	1 / 15	0.641	2 / 12	0.620
	Prompt Ensemble	2 / 102	0.962	0 / 200	0.972	0 / 15	0.654	0 / 12	0.641
	SWSA (TinyImg)	13 / 102	0.967	27 / 200	0.972	1 / 15	0.650	4 / 12	0.640
	SWSA (Diffusion)	38 / 102	0.967	64 / 200	0.973	2 / 15	0.642	1 / 12	0.614
	SWSA (CutPaste)	22 / 102	0.963	27 / 200	0.972	5 / 15	0.684	4 / 12	0.644

prompts for zero-shot image anomaly detection on real labeled validation data, which we assume is not available in our setting. Thus, we next evaluate the efficacy of SWSA in selecting CLIP prompts for our 329 anomaly detection tasks.

Zero-shot anomaly detection with CLIP. We perform zero-shot image anomaly detection with CLIP (with the ViT-B/16 backbone) as suggested by Liznerski et al. (2022); Jeong et al. (2023b): given an input image, we submit two text prompts and predict the class with the higher CLIP similarity to the image. We assume that the name of the inlier class is known. For natural image datasets, we use “some” to describe the anomaly class; for example, for the CUB dataset, if “red cardinal” is the name of the inlier class, we compare the CLIP similarities of “a photo of a red cardinal” to “a photo of some bird”. For visual anomaly datasets, we use “with defect” for anomalous images; for example, if “transistor” is the name of a product, we compare “a photo of a transistor” to “a photo of a transistor with defect”. We select amongst a

pool of ten prompt templates from Jeong et al. (2023b) for our anomaly detection tasks. A full list of candidate prompts used for each dataset can be found in Appendix B.

Evaluation setup. We evaluate each candidate prompt for the one-vs-closest and one-vs-rest settings for all 329 anomaly detection tasks, selecting the prompt with the best synthetic validation AUROC. We report both how often each strategy’s selected prompt matches the prompt selected with real validation data and the resulting AUROC for the selected prompt. For comparison, we also include two baseline strategies: (i) the default prompt template (e.g., “a photo of a [class name] bird” vs “a photo of some bird”) and (ii) a full prompt ensemble as described and suggested in Radford et al. (2021).

Evaluation results. For all four datasets, we report the best-pick rate and AUROC in Table 2. Compared to all baselines, SWSA performs best for all tasks when using diffusion-based anomalies for CUB and Flowers and when using CutPaste-based anomalies for MVTec-AD and VisA.

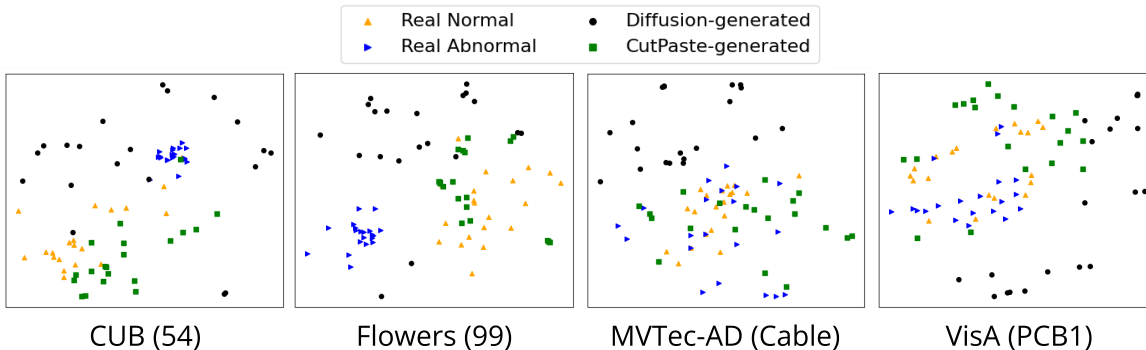


Figure 4: For each anomaly detection task, the in-class images (orange triangle), diffusion-generated anomalies (black circle), Cutpaste-generated anomalies (green square), and real one-vs-closest anomalies (blue triangle) are shown. When anomalies come from natural variations between classes (CUB and Flowers), they are better represented by diffusion-based anomalies. When anomalous images come from local changes, they are better represented by Cutpaste-based anomalies.

By selecting better prompts with our generated synthetic anomalies, we improve the zero-shot AUROC over the popular prompt ensemble, which is in fact the best prompt selection strategy for only 2 out of 329 tasks. Our generated synthetic anomalies are effective in selecting the best prompts and tuning CLIP-based anomaly detectors on various tasks, regardless of their domain or difficulty.

4.4. Qualitative Results

One assumption of our work is that validation results based on synthetic anomalies can replace validation results based on labeled ground truth validation sets. We have shown quantitatively that synthetic anomalies provide competitive model selection strategies. While it would be desirable for the synthetic anomalies to reflect the underlying true distribution of anomalies, this is not an assumption we can make: Anomalies, by definition, are too rare and the distribution of anomalies cannot be estimated in practice.

Here, we qualitatively compare the true anomalies with the artificial anomalies. Figure 4 shows a t-SNE visualization of the ViT-B-16 model’s embeddings for four different anomaly detection tasks, one from each dataset. Each plot shows the embeddings of (i) real in-class images, (ii) diffusion-based synthetic anomalies, (iii) CutPaste-based synthetic anomalies, and (iv) real anomalies. Real anomalies are not available for our method in practice, but we provide their embeddings for illustration.

When anomalies come from natural variations between classes (i.e., different species of flowers), they are further from normal data and are similar to diffusion-based anomalies. Conversely, when anomalies come from subtle, local changes (i.e., a defective pin on a chip), they are more tightly clustered around normal data and are similar to Cutpaste-based anomalies. Figure 4 shows that these ground-truth anomalies are hard to distinguish from normal data and

overlap with the normal data distribution, which makes anomaly detection with foundation models more difficult and explains why the AUROC for MVTec-AD and VisA are lower.

Shoshan et al. (2023) also study model selection with synthetic data in the binary classification setting. Their theoretical analysis also assumes that the synthetic validation data does not come from the ground truth data distribution. They show that the total variation distance between a synthetic validation set and true data provides an upper bound on the empirical risk difference between any two classifiers. We follow Sajjadi et al. (2018) in computing the total variation between synthetic and real validation datasets for our examples; details are provided in Appendix C. We find that the total variation does not provide a tight bound for synthetic validation sets with Cutpaste-based nor diffusion-based anomalies (the empirical risk difference is over 0.5 in all settings). Despite the lack of a tight bound, our empirical results in Tab. 1 show that SWSA often selects models that match selections made with a ground-truth validation set.

5. Conclusion

In this work, we propose and evaluate SWSA: an approach for selecting zero-shot anomaly detection models *without any validation data*. To substitute for a validation dataset, we propose a method that uses a general-purpose diffusion model to generate synthetic outliers, using only a small support set of in-class examples as input. Unlike prior methods for synthetic anomaly generation, we do not rely on any model training, fine-tuning, or any domain-specific architectures or techniques. Our empirical study shows that SWSA can be used with two types of synthetic anomalies (i.e., diffusion-based and Cutpaste-based synthetic anomalies) to select amongst a set of candidate models and to select prompt templates for CLIP-based zero-shot anomaly

detection. SWSA consistently outperforms common baseline strategies, such as using the largest model available or using an ensemble of prompt templates.

Impact Statement

This paper presents work whose goal is to advance the field of Machine Learning. There are many potential societal consequences of our work, none of which we feel must be specifically highlighted here.

References

- Ahmed, M., Mahmood, A. N., and Islam, M. R. A survey of anomaly detection techniques in financial domain. *Future Generation Computer Systems*, 55(C):278–288, 2016.
- Bergman, L. and Hoshen, Y. Classification-based anomaly detection for general data. In *International Conference on Learning Representations*, 2020.
- Bergman, L., Cohen, N., and Hoshen, Y. Deep nearest neighbor anomaly detection. *arXiv preprint arXiv:2002.10445*, 2020.
- Bergmann, P., Fauser, M., Sattlegger, D., and Steger, C. MVTEC AD — a comprehensive real-world dataset for unsupervised anomaly detection. In *Proceedings of the IEEE/CVF Conference on Computer Vision and Pattern Recognition*, pp. 9584–9592, 2019.
- Campos, G. O., Zimek, A., Sander, J., Campello, R. J., Míccenková, B., Schubert, E., Assent, I., and Houle, M. E. On the evaluation of unsupervised outlier detection: measures, datasets, and an empirical study. *Data mining and knowledge discovery*, 30:891–927, 2016.
- Chen, X. and Konukoglu, E. Unsupervised detection of lesions in brain MRI using constrained adversarial auto-encoders. In *MIDL Conference book*. MIDL, 2018.
- Das, S., Wong, W.-K., Dietterich, T., Fern, A., and Emmott, A. Incorporating expert feedback into active anomaly discovery. In *2016 IEEE 16th International Conference on Data Mining (ICDM)*, pp. 853–858. IEEE, 2016.
- Deecke, L., Ruff, L., Vandermeulen, R. A., and Bilen, H. Transfer-based semantic anomaly detection. In *International Conference on Machine Learning*, pp. 2546–2558. PMLR, 2021.
- Deng, J., Dong, W., Socher, R., Li, L.-J., Li, K., and Fei-Fei, L. ImageNet: A large-scale hierarchical image database. In *IEEE Conference on Computer Vision and Pattern Recognition*, pp. 248–255, 2009.
- Dhariwal, P. and Nichol, A. Diffusion models beat GANs on image synthesis. *Advances in neural information processing systems*, 34:8780–8794, 2021.
- Ding, X., Zhao, L., and Akoglu, L. Hyperparameter sensitivity in deep outlier detection: Analysis and a scalable hyper-ensemble solution. *Advances in Neural Information Processing Systems*, 35:9603–9616, 2022.
- Dosovitskiy, A., Beyer, L., Kolesnikov, A., Weissenborn, D., Zhai, X., Unterthiner, T., Dehghani, M., Minderer, M., Heigold, G., Gelly, S., Uszkoreit, J., and Houlsby, N. An image is worth 16x16 words: Transformers for image recognition at scale. In *International Conference on Learning Representations*, 2021.
- Emmott, A., Das, S., Dietterich, T., Fern, A., and Wong, W.-K. A meta-analysis of the anomaly detection problem. *arXiv preprint arXiv:1503.01158*, 2015.
- Esmaeilpour, S., Liu, B., Robertson, E., and Shu, L. Zero-shot out-of-distribution detection based on the pretrained model CLIP. In *Proceedings of the AAAI conference on artificial intelligence*, 2022.
- Fernando, T., Gammulle, H., Denman, S., Sridharan, S., and Fookes, C. Deep learning for medical anomaly detection—a survey. *ACM Computing Surveys*, 54(7):1–37, 2021.
- Goldstein, M. and Uchida, S. A comparative evaluation of unsupervised anomaly detection algorithms for multivariate data. *PloS one*, 11(4):e0152173, 2016.
- Görnitz, N., Kloft, M., Rieck, K., and Brefeld, U. Toward supervised anomaly detection. *Journal of Artificial Intelligence Research*, 46:235–262, 2013.
- Han, S., Hu, X., Huang, H., Jiang, M., and Zhao, Y. AD-Bench: Anomaly detection benchmark. *Advances in Neural Information Processing Systems*, 35:32142–32159, 2022.
- He, K., Zhang, X., Ren, S., and Sun, J. Deep residual learning for image recognition. In *Proceedings of the IEEE conference on Computer Vision and Pattern Recognition*, pp. 770–778, 2016.
- Hendrycks, D., Mazeika, M., and Dietterich, T. Deep anomaly detection with outlier exposure. In *International Conference on Learning Representations*, 2019a.
- Hendrycks, D., Mazeika, M., Kadavath, S., and Song, D. Using self-supervised learning can improve model robustness and uncertainty. *Advances in Neural Information Processing Systems*, 32:15663–15674, 2019b.
- Ho, J., Jain, A., and Abbeel, P. Denoising diffusion probabilistic models. *Advances in Neural Information Processing Systems*, 33:6840–6851, 2020.

- Jain, S., Lawrence, H., Moitra, A., and Madry, A. Distilling model failures as directions in latent space. In *International Conference on Learning Representations*, 2023.
- Jeong, J., Kwon, M., and Uh, Y. Training-free style transfer emerges from h-space in diffusion models. *arXiv preprint arXiv:2303.15403*, 2023a.
- Jeong, J., Zou, Y., Kim, T., Zhang, D., Ravichandran, A., and Dabeer, O. WinCLIP: Zero-/few-shot anomaly classification and segmentation. In *Proceedings of the IEEE/CVF Conference on Computer Vision and Pattern Recognition*, pp. 19606–19616, 2023b.
- Karras, T., Laine, S., and Aila, T. A style-based generator architecture for generative adversarial networks. In *Proceedings of the IEEE/CVF Conference on Computer Vision and Pattern Recognition*, pp. 4401–4410, 2019.
- Karras, T., Laine, S., Aittala, M., Hellsten, J., Lehtinen, J., and Aila, T. Analyzing and improving the image quality of StyleGAN. In *Proceedings of the IEEE/CVF Conference on Computer Vision and Pattern Recognition*, pp. 8110–8119, 2020.
- Kawar, B., Zada, S., Lang, O., Tov, O., Chang, H., Dekel, T., Mosseri, I., and Irani, M. Imagic: Text-based real image editing with diffusion models. In *Proceedings of the IEEE/CVF Conference on Computer Vision and Pattern Recognition*, pp. 6007–6017, 2023.
- Kim, G., Kwon, T., and Ye, J. C. DiffusionCLIP: Text-guided diffusion models for robust image manipulation. In *Proceedings of the IEEE/CVF Conference on Computer Vision and Pattern Recognition*, pp. 2426–2435, 2022.
- Kwon, M., Jeong, J., and Uh, Y. Diffusion models already have a semantic latent space. In *International Conference on Learning Representations*, 2023.
- Li, A., Qiu, C., Kloft, M., Smyth, P., Mandt, S., and Rudolph, M. Deep anomaly detection under labeling budget constraints. In *International Conference on Machine Learning*, pp. 19882–19910. PMLR, 2023a.
- Li, A., Qiu, C., Kloft, M., Smyth, P., Rudolph, M., and Mandt, S. Zero-shot anomaly detection without foundation models. *arXiv preprint arXiv:2302.07849*, 2023b.
- Li, C.-L., Sohn, K., Yoon, J., and Pfister, T. Cutpaste: Self-supervised learning for anomaly detection and localization. In *Proceedings of the IEEE/CVF conference on Computer Vision and Pattern Recognition*, pp. 9664–9674, 2021.
- Liznerski, P., Ruff, L., Vandermeulen, R. A., Franks, B. J., Muller, K. R., and Kloft, M. Exposing outlier exposure: What can be learned from few, one, and zero outlier images. *Transactions on Machine Learning Research*, 2022.
- Luo, J., Wang, Z., Wu, C. H., Huang, D., and De la Torre, F. Zero-shot model diagnosis. In *Proceedings of the IEEE/CVF Conference on Computer Vision and Pattern Recognition*, pp. 11631–11640, 2023.
- Ma, M. Q., Zhao, Y., Zhang, X., and Akoglu, L. The need for unsupervised outlier model selection: A review and evaluation of internal evaluation strategies. *ACM SIGKDD Explorations Newsletter*, 25(1), 2023.
- Marques, H. O., Campello, R. J., Zimek, A., and Sander, J. On the internal evaluation of unsupervised outlier detection. In *Proceedings of the 27th international conference on scientific and statistical database management*, pp. 1–12, 2015.
- Marques, H. O., Campello, R. J., Sander, J., and Zimek, A. Internal evaluation of unsupervised outlier detection. *ACM Transactions on Knowledge Discovery from Data (TKDD)*, 14(4):1–42, 2020.
- Maxion, R. and Tan, K. Benchmarking anomaly-based detection systems. In *International Conference on Dependable Systems and Networks*, pp. 623–630, 2000.
- Mirsky, Y., Doitshman, T., Elovici, Y., and Shabtai, A. Kitsune: an ensemble of autoencoders for online network intrusion detection. In *Network and Distributed System Security Symposium*, 2018.
- Mirzaei, H., Salehi, M., Shahabi, S., Gavves, E., Snoek, C. G. M., Sabokrou, M., and Rohban, M. H. Fake it until you make it: Towards accurate near-distribution novelty detection. In *International Conference on Learning Representations*, 2023.
- Mokady, R., Hertz, A., Aberman, K., Pritch, Y., and Cohen-Or, D. Null-text inversion for editing real images using guided diffusion models. In *Proceedings of the IEEE/CVF Conference on Computer Vision and Pattern Recognition*, pp. 6038–6047, 2023.
- Nguyen, T. T., Nguyen, U. Q., et al. An evaluation method for unsupervised anomaly detection algorithms. *Journal of Computer Science and Cybernetics*, 32(3):259–272, 2016.
- Nilsback, M.-E. and Zisserman, A. Automated flower classification over a large number of classes. In *Indian Conference on Computer Vision, Graphics and Image Processing*, 2008.

- Principi, E., Vesperini, F., Squartini, S., and Piazza, F. Acoustic novelty detection with adversarial autoencoders. In *2017 International Joint Conference on Neural Networks (IJCNN)*, pp. 3324–3330. IEEE, 2017.
- Qiu, C., Pfrommer, T., Kloft, M., Mandt, S., and Rudolph, M. Neural transformation learning for deep anomaly detection beyond images. In *International Conference on Machine Learning*, pp. 8703–8714. PMLR, 2021.
- Qiu, C., Kloft, M., Mandt, S., and Rudolph, M. Raising the bar in graph-level anomaly detection. In *Proceedings of the Thirty-First International Joint Conference on Artificial Intelligence, IJCAI-22*, pp. 2196–2203, 2022a.
- Qiu, C., Li, A., Kloft, M., Rudolph, M., and Mandt, S. Latent outlier exposure for anomaly detection with contaminated data. In *International Conference on Machine Learning*, pp. 18153–18167. PMLR, 2022b.
- Radford, A., Kim, J. W., Hallacy, C., Ramesh, A., Goh, G., Agarwal, S., Sastry, G., Askell, A., Mishkin, P., Clark, J., et al. Learning transferable visual models from natural language supervision. In *International Conference on Machine Learning*, pp. 8748–8763, 2021.
- Reiss, T., Cohen, N., Bergman, L., and Hoshen, Y. Panda: Adapting pretrained features for anomaly detection and segmentation. In *Proceedings of the IEEE/CVF Conference on Computer Vision and Pattern Recognition*, pp. 2806–2814, 2021.
- Ruff, L., Vandermeulen, R., Goernitz, N., Deecke, L., Siddiqui, S. A., Binder, A., Müller, E., and Kloft, M. Deep one-class classification. In *International conference on machine learning*, pp. 4393–4402. PMLR, 2018.
- Ruff, L., Vandermeulen, R. A., Görnitz, N., Binder, A., Müller, E., Müller, K.-R., and Kloft, M. Deep semi-supervised anomaly detection. In *International Conference on Learning Representations*, 2019.
- Sajjadi, M. S., Bachem, O., Lucic, M., Bousquet, O., and Gelly, S. Assessing generative models via precision and recall. *Advances in neural information processing systems*, 31, 2018.
- Schneider, T., Qiu, C., Kloft, M., Latif, D. A., Staab, S., Mandt, S., and Rudolph, M. Detecting anomalies within time series using local neural transformations. *arXiv preprint arXiv:2202.03944*, 2022.
- Schubert, D., Gupta, P., and Wever, M. Meta-learning for automated selection of anomaly detectors for semi-supervised datasets. In *International Symposium on Intelligent Data Analysis*, pp. 392–405. Springer, 2023.
- Shoshan, A., Bhonker, N., Kviatkovsky, I., Fintz, M., and Medioni, G. Synthetic data for model selection. In *Proceedings of the 40th International Conference on Machine Learning*, pp. 31633–31656, 2023.
- Siadati, H. and Memon, N. Detecting structurally anomalous logins within enterprise networks. In *Proceedings of the 2017 ACM SIGSAC Conference on Computer and Communications Security*, pp. 1273–1284, 2017.
- Sohn, K., Li, C.-L., Yoon, J., Jin, M., and Pfister, T. Learning and evaluating representations for deep one-class classification. In *International Conference on Learning Representations*, 2020.
- Song, J., Meng, C., and Ermon, S. Denoising diffusion implicit models. In *International Conference on Learning Representations*, 2021.
- Trittenbach, H., Englhardt, A., and Böhm, K. An overview and a benchmark of active learning for outlier detection with one-class classifiers. *Expert Systems with Applications*, 168:114372, 2021.
- Tumanyan, N., Geyer, M., Bagon, S., and Dekel, T. Plug-and-play diffusion features for text-driven image-to-image translation. In *Proceedings of the IEEE/CVF Conference on Computer Vision and Pattern Recognition*, pp. 1921–1930, 2023.
- Wah, C., Branson, S., Welinder, P., Perona, P., and Belongie, S. The Caltech-UCSD Birds-200-2011 Dataset. Technical Report CNS-TR-2011-001, California Institute of Technology, 2011.
- Zhao, Y., Rossi, R., and Akoglu, L. Automatic unsupervised outlier model selection. *Advances in Neural Information Processing Systems*, 34:4489–4502, 2021.
- Zhao, Y., Zhang, S., and Akoglu, L. Toward unsupervised outlier model selection. In *2022 IEEE International Conference on Data Mining (ICDM)*, pp. 773–782. IEEE, 2022.
- Zhou, C., Loy, C. C., and Dai, B. DenseCLIP: Extract free dense labels from CLIP. *arXiv preprint arXiv:2112.01071*, 2021.
- Zou, Y., Jeong, J., Pemula, L., Zhang, D., and Dabeer, O. Spot-the-difference self-supervised pre-training for anomaly detection and segmentation. In *European Conference on Computer Vision*, pp. 392–408, 2022.

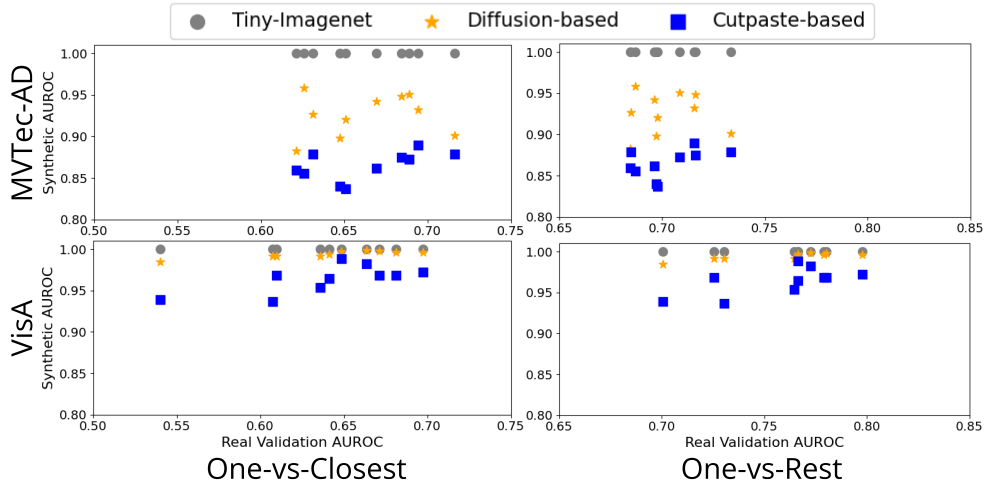


Figure 5: We compare the real and synthetic validation AUROC when performing model selection for the MVTec-AD and VisA datasets. We find that the trends are weaker than with natural-image datasets (i.e., CUB and Flowers), and neither diffusion-based or Cutpaste-based anomalies preserve the true model ranking on these datasets.

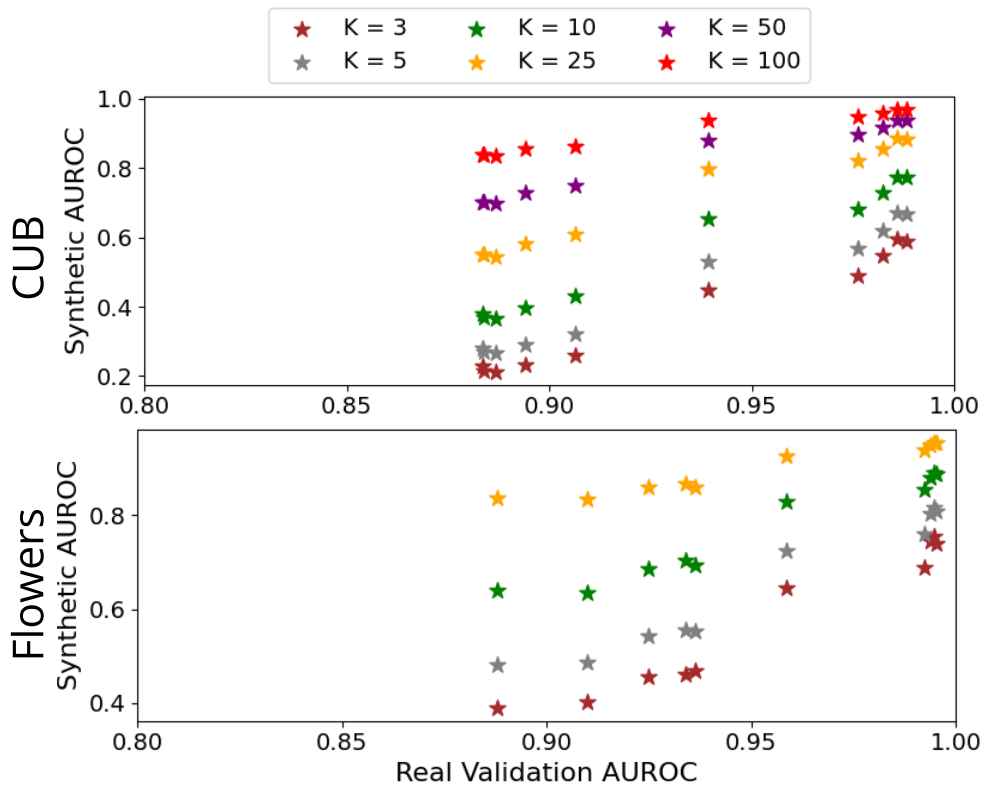


Figure 6: We compare the real and synthetic validation AUROC when performing model selection with fewer synthetic anomalies, for the one-vs-rest benchmark on the CUB and Flowers datasets. We find that, although the performance in general is worse when fewer synthetic anomalies are used, the error ranking is still largely preserved, even when only three synthetic anomalies are used ($K = 3$).

A. Additional Results

Additional MVTec-AD and VisA results. Figure 5 shows the results of the model selection experiment with the MVTec-AD and VisA datasets on the one-vs-closest and the one-vs-rest benchmarks. Unlike the CUB and Flowers datasets, in which synthetic anomalies could successfully approximate real validation performance, our synthetic anomalies are less effective for these datasets.

We also comment on the performance of our method when selecting CLIP prompts for MVTec-AD. We noticed a disparity in performance between objects in MVTec-AD (e.g., capsules, cables, or screws) and textures in MVTec-AD (e.g., carpets, wood, or tiles). Our method is unable to select the best CLIP prompt in any of the six textures for MVTec-AD, instead only performing relatively better on the MVTec-AD objects. We therefore identify yet another challenge when using our approach for industrial anomaly detection—DiffStyle relies on assumptions of “style” and “content” in their source images, and these elements are not present in MVTec-AD textures like carpets or tiles.

Results with fewer synthetic anomalies. Figure 6 shows the model ranking performance for CUB and Flowers with diffusion-based synthetic anomalies on the one-vs-rest benchmark, which is the best-performing setting in our evaluation. We vary K , the number of synthetic anomalies are used, from 100 to as few as 3. Our evaluation shows that, even though the overall performance drops when fewer synthetic anomalies are used, the model ranking stays relatively consistent.

B. CLIP prompt templates

For our experiments in Sec. 4.3, we evaluated across set of ten candidate prompt templates. Our evaluated prompts are general-purpose, and only the term “bird” or “flower” is added to the template for the CUB and Flowers dataset respectively. Unlike the techniques used in Jeong et al. (2023b), we do not perform any special class-specific modifications for any classes or products. Only mild class-name cleaning is performed: we remove trailing numbers from class names and fully write all acronyms (e.g., “PCB1” becomes “printed circuit board”). For each dataset, the candidate prompt templates are provided below:

```
% CLIP Templates for Flowers
['a photo of a {} flower', 'a photo of some flower'],
['a cropped photo of a {} flower', 'a cropped photo of some flower'],
['a dark photo of a {} flower', 'a dark photo of some flower'],
['a photo of a {} flower for inspection', 'a photo of some flower for inspection'],
['a photo of a {} flower for viewing', 'a photo of some flower for viewing'],
['a bright photo of a {} flower', 'a bright photo of some flower'],
['a close-up photo of a {} flower', 'a close-up photo of some flower'],
['a blurry photo of a {} flower', 'a blurry photo of some flower'],
['a photo of a small {} flower', 'a photo of a small some flower'],
['a photo of a large {} flower', 'a photo of a large some flower'],
```

```
% CLIP Templates for CUB
['a photo of a {} bird', 'a photo of some bird'],
['a cropped photo of a {} bird', 'a cropped photo of some bird'],
['a dark photo of a {} bird', 'a dark photo of some bird'],
['a photo of a {} bird for inspection', 'a photo of some bird for inspection'],
['a photo of a {} bird for viewing', 'a photo of some bird for viewing'],
['a bright photo of a {} bird', 'a bright photo of some bird'],
['a close-up photo of a {} bird', 'a close-up photo of some bird'],
['a blurry photo of a {} bird', 'a blurry photo of some bird'],
['a photo of a small {} bird', 'a photo of a small some bird'],
['a photo of a large {} bird', 'a photo of a large some bird'],
```

```
% CLIP Templates for MVTec-AD and VisA
['a photo of a {}', 'a photo of a {} with defect'],
['a cropped photo of a {}', 'a cropped photo of a {} with defect'],
['a dark photo of a {}', 'a dark photo of a {} with defect'],
['a photo of a {} for inspection', 'a photo of a {} with defect for inspection'],
['a photo of a {} for viewing', 'a photo of a {} with defect for viewing'],
['a bright photo of a {}', 'a bright photo of a {} with defect'],
['a close-up photo of a {}', 'a close-up photo of a {} with defect'],
['a blurry photo of a {}', 'a blurry photo of {} with defect'],
['a photo of a small {}', 'a photo of a small {} with defect'],
['a photo of a large {}', 'a photo of a large {} with defect'],
```

Table 3: Total variation for the example classes shown in Figure 4. We find that, despite our empirical results, no setting provides a tight bound, and we cannot strong guarantees on rank preservation on anomaly detection tasks.

	Flowers	CUB	MVTec-AD	VisA
Total variation: Real validation set vs Diffusion-based validation set	0.698	1.257	1.143	0.934
Total variation: Real validation set vs CutPaste-based validation set	0.697	1.042	0.534	0.804

C. Total variation results

To compute total variation, we follow the methodology of Sajjadi et al. (2018) to compute total variation: given two datasets D_1, D_2 , we convert them to their embeddings and perform a k-means clustering on their union $F(D_1) \cup F(D_2)$. Each all point is assigned to a cluster $y \in \{0 \dots k\}$, and we separate the cluster assignments into Y_1 and Y_2 based on their original datasets. We then use the histogram of their corresponding cluster assignments to compute the total variation: $TV = \sum_i |K_{i,1} - K_{i,2}|$, where $K_{i,j}$ returns the number of points assigned to cluster i in dataset j . As a heuristic, we use $k = \sqrt{|D_1| + |D_2|}$ clusters when computing the total variation, and report the average of ten k-means initializations.

When computing the total variation between validation datasets, we let $D_1 = X_{\text{support}} \cup X_{\text{out}}$ and $D_2 = X_{\text{support}} \cup \tilde{X}_{\text{out}}$, where \tilde{X}_{out} are the synthetic anomalies produced by our diffusion-based or CutPaste-based method. The total variation calculation results are shown in Table 3.